Eur. Phys. J. Spec. Top. (2023) 232:499–508
https://doi.org/10.1140/epjs/s11734-023-00810-y

THE EUROPEAN PHYSICAL JOURNAL SPECIAL TOPICS

Regular Article

Isolated wave segments in a neural tissue model with volume transmission: discreteness matters

Andrey Yu. Verisokin[1,a], Darya V. Verveyko[1,b], and Dmitry E. Postnov[2,c]

[1] Department of Theoretical Physics, Kursk State University, Radishcheva st., 33, 305000 Kursk, Russia
[2] Department of Optics and Biophotonics, Saratov State University, Astrakhanskaya st., 83, 410012 Saratov, Russia

Received 1 February 2023 / Accepted 9 March 2023 / Published online 24 March 2023

Abstract Isolated wave segments are a type of spatiotemporal activity that has been repeatedly reported in experimental studies of spreading depolarization on the cerebral cortex and retina of laboratory animals. However, it has been theoretically shown that such a pattern cannot be stable in a continuous excitable medium. In our work, we address this problem using the model of a discrete–continuous medium. We present the targeted numerical study of isolated wave segments, including scenarios of their emergence and an estimation of their stability to various deformations. We show that an isolated wave segment can exhibit the properties of a space-time attractor by cyclically changing its shape and approaching it from different initial conditions. Such a wave segment is not necessarily small, although small segments may occur more easily and are, therefore, more likely. Finally, we show that the behavior we found persists also under conditions of a heterogeneous propagation medium, which indicates the applicability of our findings to the analysis of spatiotemporal patterns in real nervous tissue.

1 Introduction

Spreading depolarization (SD) is an extreme state of the nervous tissue of the brain that occurs with cortical spreading depression, migraine, and brain injury [1–3]. Since the discovery of cortical spreading depression in 1944 [4], mathematical models of various levels of detail have been proposed. Since the SD propagation mechanism relies on the diffusion of substances in the intercellular space, models of a continuous active medium with diffusion have become a very expected modeling paradigm [5–11].

Observation of SD in the brains of laboratory animals reveals rich spatiotemporal dynamics, including spiral and radial waves, retracting waves, and isolated wave segments [12–14]. If the first three types of activity are well described by models of active media, then with the fourth—isolated wave segments—the situation is not completely clear.

There are the multiple reports on isolated wave segments in real life [15–18]. However, for basic models of excitable media, it was proved that an isolated wave segment is unstable by nature, it must either collapse or develop into a spiral wave [19, 20]. It is very difficult to verify the validity of this statement for real brain tissue due to insufficient observation time, limited propagation space, and an unknown degree of heterogeneity in the properties of nervous tissue. Therefore, it is possible that the instability of isolated wave segments is more a property of the chosen model than of the object under consideration.

The structure of the cerebral cortex (as well as other tissues of a living organism), on the one hand, has a number of continuous characteristics that provide the general properties of a functioning system as a whole, and on the other hand, it is composed of cells as discrete elements, this empowers to consider cerebral cortex both as a continuous and as a discrete medium. Such a medium transmits electrical signals like a set of discrete elements for which the model description in the form of a continuous medium is not suitable. At the same time, the notion of a continuous porous medium is well applicable for the intercellular space, in which the exchange of substances between cells occurs. The question of the combination of discreteness and continuity in models was discussed, for example, in [21, 22].

Usually, the choice of the type of mathematical model is limited by the available experimental data to compare with and target effects it should reproduce. For example, if information about neuronal activity is obtained

Brain Physiology Meets Complex Systems. Guest editors: Thomas Penzel, Teemu Myllylä, Oxana V. Semyachkina-Glushkovskaya, Alexey Pavlov, Anatoly Karavaev.

[a] e-mail: ffalconn@mail.ru
[b] e-mail: allegroform@mail.ru
[c] e-mail: postnov@info.sgu.ru (corresponding author)

by extracellular recording and, therefore, involves averaging over a certain area, then a model in the form of a continuous active medium will be very suitable, since the recording electrode can be placed in any of the available locations and, with its small displacement, the characteristics of the recorded signal will also change a little. However, for a thin layer of neuron culture, we will see a different picture, when within one cell the electric potential is almost the same, but differs greatly from the recording from a neighboring cell. Obviously, in this case, a spatially discrete model, consisting of individual elements and connections between them, will be more adequate. One neurovascular unit [23] of the brain parenchyma has 40–60 microns in the crossbar, so there are only about 20 of them on a distance of one millimeter. In this case, the continuous active medium model does not look like the best choice, since, for example, it is not able to describe the uncorrelated firing of neighboring neurons. In search of a better model description, it is appropriate to consider models in which neurons are discrete but connected in a way, which (but not neurons!) approximates a continuous medium.

In our work, we study the behavior of isolated wave segments using the model previously proposed in the works [24–26]. In particular, in [26] it was observed that as a result of a short-term noise burst, many wave segments are born, of which the smallest few survive the longest. Here we present the targeted numerical study of such long-living wave segments, including scenarios of their emergence and an estimation of their stability to various deformations. We show that an isolated wave segment exhibits the properties of a space-time attractor by cyclically changing its shape and approaching it from different initial conditions. Therefore, throughout the text, we refer to them as stable wave segments (SWS). Such a wave segment is not necessarily small, although small segments may occur more easily and are, therefore, more likely. Finally, we show that the behavior we found persists also under conditions of a heterogeneous propagation medium, that indicates the applicability of our findings to the analysis of spatiotemporal patterns in real nervous tissue.

In Discussion we argue that, similarly to a continuous medium, the stability of isolated wave segment is determined by events at its edge, while the central part can have any length, tending in shape to a plane wave as its size increases.

2 Model

2.1 Spatial structure

In real tissue of the brain parenchyma, cells have different shapes and sizes and are arranged in an irregular manner, see for illustrations [27, 28]. Such an arrangement is schematically reproduced in Fig. 1a, where a section of nervous tissue is depicted. When creating a computational model, in the first step, we simplify the irregular cell placement in a real tissue to a regular arrangement of neurons in extracellular space (ECS), as shown in Fig. 1b. It is convenient to use a two-dimensional grid, each point (pixel) of which is associated with one cell and the volume of the ECS assigned to it, see Fig. 1c. Thus, we consider the activity of discrete set of units-neurons, while the connection between them is carried out through a continuous layer that represents the ECS.

2.2 Local dynamics

We based on the extension of the FitzHugh–Nagumo model previously proposed in [24, 25], where the equations for fast spiking variable u and slow recovery variable ν, are supplied with the equation for the extracellular potassium concentration z:

$$\varepsilon_u \frac{\partial u}{\partial t} = u - \frac{u^3}{3} - \nu + F(u,z) + D\xi(x,y,t), \quad (1)$$

$$\varepsilon_\nu(u) \frac{\partial \nu}{\partial t} = au + b - \nu, \quad (2)$$

$$\varepsilon_z \frac{\partial z}{\partial t} = \alpha_z \psi(u) - z + \gamma_z z_{diff}(x,y). \quad (3)$$

Parameters a and b in (2) control position of ν-nullcline (see the red line in Fig. 2a). Equations (1)–(2) themselves without the term $F(u, z)$ describe a purely discrete medium. However, we transform the model to present a realistic biophysical approach. We introduce a variable z (see [26]) that describes the changes of the extracellular potassium concentration. In turn, the characteristics of ECS depend on z value. Thereby we can simplistically consider that z variable determines the ECS size, i.e., the distances between discrete elements of the model medium. In other words, the variable z makes the medium discrete–continuous. We define the term $F(u, z)$ in the following way: $F(u, z) = z(a_1 - a_2(1 - u)^m)$. The nullclines for $z = 0$ and $z = 1$ values are shown in Fig. 2a (the solid and dotted blue lines correspondingly). The term $D\xi(x, y, t)$ stands for Gaussian noise with intensity D which represents the random-like total postsynaptic stimulus received by a neuron.

The nonlinear function

$$\psi(u) = 0.5(1 + \tanh(u/u_s)) \quad (4)$$

accounts for potassium release. Function $\psi(u)$ is equal to zero in the rest state and tends to unit value as u increases.

The term $\gamma_z z_{diff}(x, y)$ describes the redistribution of z over available ECS by means of diffusion. Diffusion of z variable is simulated in terms of the finite-element approximation of the concentration flows between the neighboring pixels:

$$z_{diff}(x,y) = \left(\sum_{nb} z_{i,j} - 4z_{x,y} \right), \quad (5)$$

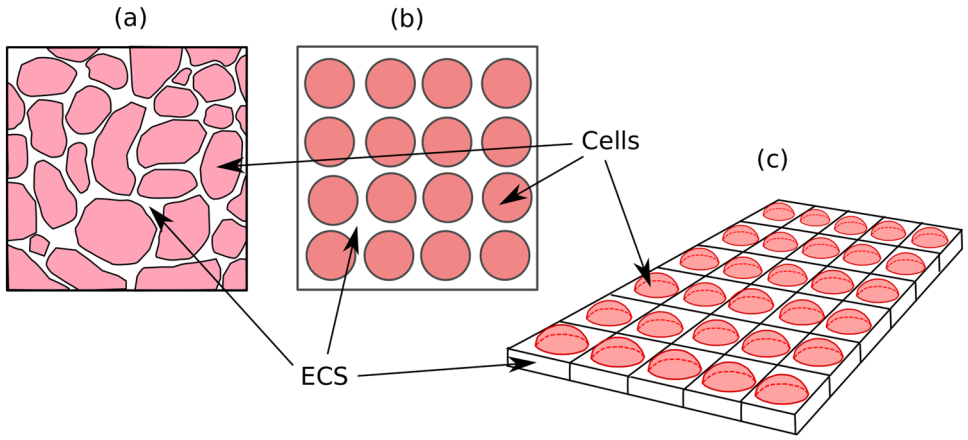

Fig. 1 Transition from a realistic topology of the ECS to a 2D grid in the model. **a** A typical picture in a tissue section; **b** a regularized representation of a flat structure; **c** ECS (white) forms the continuous layer, while the active elements-neurons are disconnected

where nb denotes all combinations of (i, j) that are adjacent to location (x, y).

In order to implement different time scales for spike generation and recovery stage, function $\varepsilon_\nu(u)$ takes two different values: τ_{spike} if $u > 0$ and τ_{rest} otherwise. Thus, ε_ν is

$$\varepsilon_\nu(u) = \tau_{spike}(1 - \psi(u)) + \tau_{rest}\psi(u). \qquad (6)$$

In the absence of neural spikes, when $\psi(u) = 0$ and $z \longrightarrow 0$ (bottom plane in Fig. 2), the dynamics of the subsystem (1)–(2) is the same as for the conventional FitzHugh–Nagumo model. In the presence of spikes that activate z in (3) by means of (4), the dynamics of the system demonstrates both excitability and bistability [24]: at rare spiking events the trajectory returns to the initial point EQP 1, while the intensive and long enough stimulus can trigger the transition to self-sustained oscillations (the schematically shown orbit LC) or (at higher α_z) to the EQP 2.

2.3 Numeric methods

The set of equations (1)–(3) was integrated numerically by the explicit method (the fourth-order Runge–Kutta method adopted for SDE [29–31]). The numerical algorithm to perform such simulations was chosen according to parallel computing needs [32].

In order to assess the long-term stability of the SWSs, we construct the solution domain of the toroidal shape. It was done simply by connection between the left and right boundaries, and between the upper and lower boundaries of the 2D lattice. This method does not take into account the surface curvature effects studied in [33], but fits well our specific needs, providing the unbounded uniform propagation space for a single SWS.

In order to quantify wave segments under study, we assumed that only pixels in which $z > z_{th}$ belongs to the segment, where $z_{th} > 0$ is the empirically determined threshold value. Then, we determined segment size in pixels and calculated three quantities S_u, S_v, and S_z as the total sums of deviations u, ν, z from its rest values over the segment area, $S_u = \sum(u - u_0)$, $S_v = \sum(v - v_0)$, $S_z = \sum(z - z_0)$. Note, the specific choice of z_{th} strongly affects the segment size, but not S_u, S_v, S_z. In our work we take z_{th} equal to 0.01. The rest values: $u_0 = -1.0576$, $v_0 - 0.6633$, $z_0 = 0$.

To quantify the motion of wave segments we calculated the velocity V_s as the number of pixels that a segment passes per a unit of dimensionless time.

The program code and the datasets used in Figs. 3 are available as Supplemental Material. The set of model parameters is given in Table 1.

3 Results

3.1 Scenarios of origin

Previously, it was demonstrated that SWS can emerge spontaneously under the short-term excitation by a spatially uncorrelated noise burst which triggers the variety of excitation clusters [26]. After the noise burst ends, (i) large patterns become the growing waves; (ii) small patterns disappear; (iii) some suitable patterns take the form of wave segments that survive for a long time and looks stable in size. An example is provided in the Supplemental Material (see SWS_Emergence_Scenario_1 - Noise.avi).

Here, we present three examples of deterministic medium leading to SWS formation, see Fig. 3. For each of the figure panels, numbers 1, 2, 3 indicate the sequence of time moments when snapshots were taken. Video files with detailed descriptions and files with the initial conditions (.st and .gif files) of the solutions in Fig. 3b, c can be found in Supplemental Material.

Figure 3a shows the propagation of the plane wave through the "wall" (Dirichlet boundary condition $z = 0$, shown as yellow line) with three gaps of different sizes—3, 8 and 20 pixels wide. Easy to see that small gap does not allow the wave propagation at all, too large gap leads to the formation of the growing wave front, while some appropriate gap (in the middle) provide the formation of small wave segment with seemingly constant size.

Table 1 The set of parameter values for the model (1)–(3)

ε_u	τ_{spike}	τ_{rest}	ε_z	a_1	b	D
0.04	1.5	1.0	0.5	1	0.5	0.005
α_z	a_2	a	γ_z	u_s	m	
0.75	0.06	1.1	0.5	0.05	3	

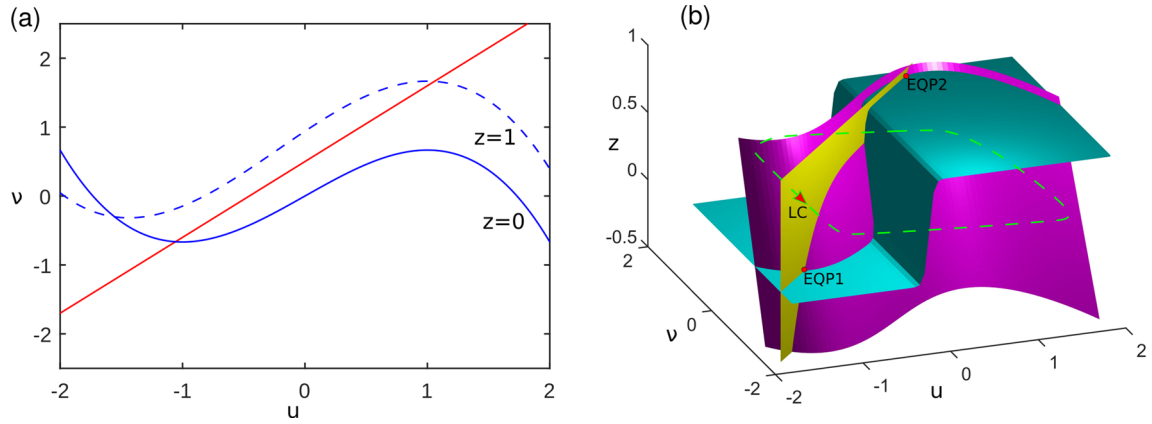

Fig. 2 Nullcline plot for a single unit defined by the Eqs. (1)–(3). **a** Nullclines $\nu(u)$ for the equations (1)–(2). **b** Three nullcline surfaces are defined by the conditions $\frac{\partial u}{\partial t} = 0$ (magenta), $\frac{\partial \nu}{\partial t} = 0$ (yellow), and $\frac{\partial z}{\partial t} = 0$ (cyan)

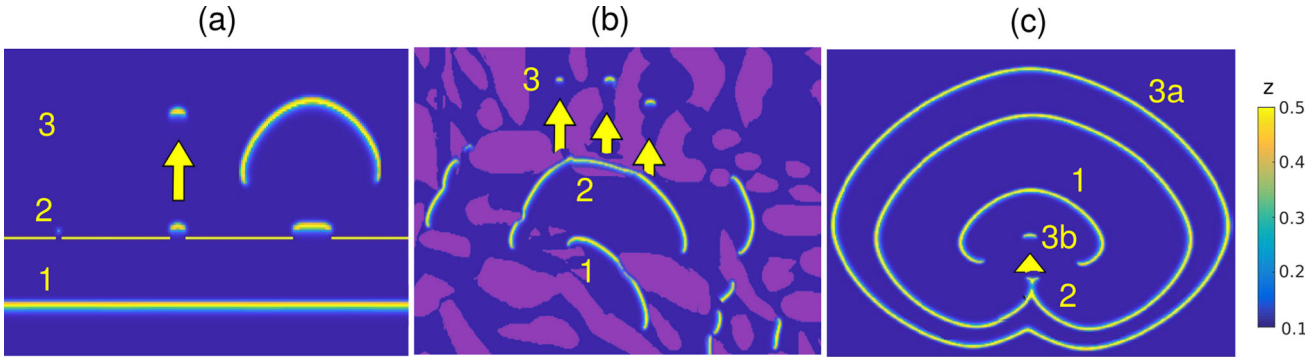

Fig. 3 Deterministic SWS formation scenarios: **a** a plane wave passes through gaps in Dirichlet boundary, **b** a wave front spreads through an inhomogeneous medium with variable γ_z ($\varepsilon_z = 0.6$, $\gamma_z = 0.25$ and $\gamma_z = 0.5$ in violet and blue areas, respectively), **c** as a result of the approach and collision of two curling ends of the same growing wave. For all three panels SWSs are marked with yellow arrows. The numbers show the evolution of the front in three successive time moments. In **c** two structures appeared simultaneously are marked with the letters a and b. See also video illustrations of the process in Supplemental Material

Figure 3b demonstrates the emergence of SWS when growing wave passes through an inhomogeneous medium containing regions with reduced diffusion rate ($\gamma_z = 0.25$ in contrast to the $\gamma_z = 0.5$ in the rest part of medium.

Figure 3c shows the formation of SWS by collision of two curling ends of the same growing wave front. Similarly, SWS can emerge in collision of the ends from two different wave fronts (see the video in Supplemental Material).

Summarizing, the formation of small long-living wave segments is not an exception, at least for the active medium under consideration. The examples above naturally raise the question of the mechanism of spontaneous SWS generation and, in particular, why do only small segments become long-lived? We will return to this issue in the Discussion based on the results shown in the following sections. Below we study the features of already existing SWS disregarding the way of it formation.

3.2 Traveling SWS features

Figure 4a shows a specific SWS that we consider below. It can be seen that the object is better localized by the

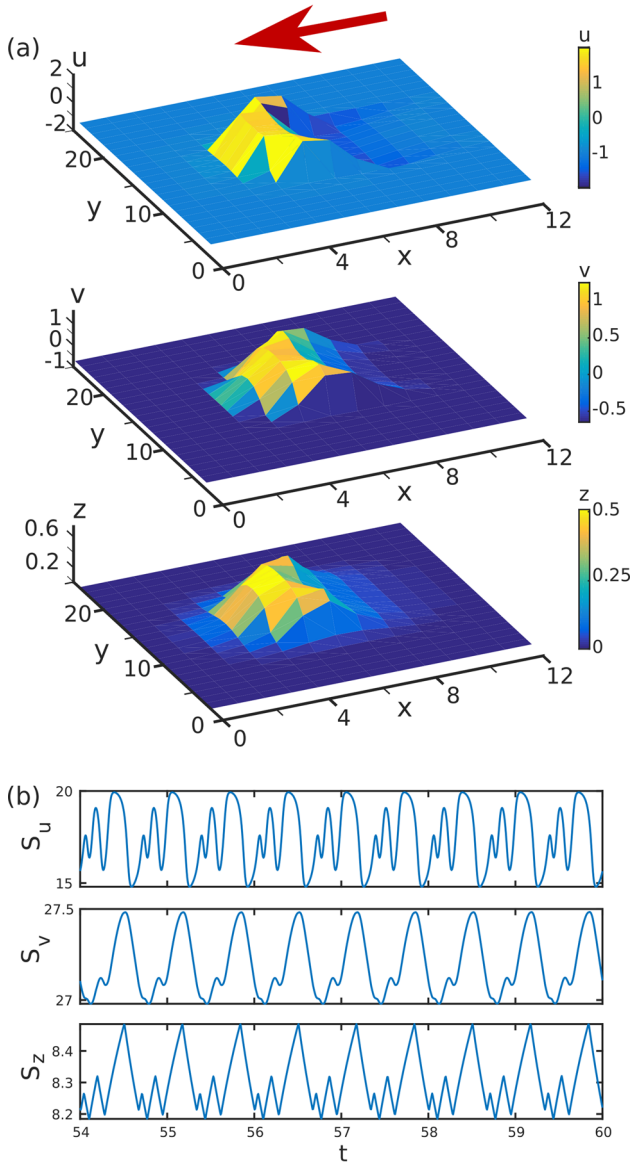

Fig. 4 **a** The 2D profiles of variables u, ν and z in SWS at the selected time moment; **b** time courses of S_u, S_v, S_z show oscillations

variables u, ν than by the variable z, which provides a spatial coupling.

The main feature of SWS is their indefinitely long time living without growing or collapsing. However, this does not mean that their shape and size are constant over time. Figure 4b, c shows the details. While moving, the SWS change its shape according to a specific scenario. In order to characterize this motion, panel (b) shows the time courses of S_u, S_v, S_z. It can be seen that each of these quantities shows oscillations, and their combined change gives a closed orbit, shown in panel (c). Thus, phenomenologically, SWS is similar to the object known as breathing dissipative solitons, which have recently attracted the attention of researchers in nonlinear optics. [34, 35].

Below we analyze the features of SWS motion and evolution, depending on its size and shape.

3.3 SWS is resistant to small deformations

The closed orbit in Fig. 4c resembles a limit cycle in low-dimensional dissipative systems. To test this hypothesis, we introduce small deviations and follow their evolution.

As initial conditions, we take the distribution of u, ν, z from Fig. 4a. At first, we take an initially large area. We assign stationary values u_0, v_0, z_0 to the variables at each area point. Then, we take the SWS (i.e., the variable distributions) from Fig. 4a and scale this structure by S_k times using the linear interpolation method. Further, if there are no additional instructions, it should be considered that the scaling by S_k times is performed only in one direction—perpendicular to the direction of motion. We interpolate u, ν, z values according to S_k value and put new distributions on the previously created area of stationary values for further numerical simulations. Therefore, we get a new area with a new scaled SWS inside.

Figure 5 shows the results for scaling rate $S_k = 0.8$ (b) in respect to the original shape at $S_k = 1.0$ (a). With tiny but visible differences at $t = 0.1$, both cases converges to the same shape by the time $t = 10$. Figure 5c shows the process in terms of S_u, S_v, S_z.It reveals the complex transient that converges to the closed orbit shown in Fig. 4c and marked by green in Fig. 5c.

Regardless of the formation scenario, the emerging SWSs move strictly vertically or horizontally on the 2D grid. We used the rotation of the template from Fig. 4 as another way to set the initial perturbation. The results are shown in Fig. 6.

Panel (a) shows how the rotation of the original structure by 45° leads to the rapidly growth of the structure, moving at an angle to the vertical. At smaller angle of rotation (10°) SWS rapidly turns around tending to its original form (Fig. 6b).

The performed targeted set of simulations shows that any structures with the front moving with a sufficiently large inclination to the vertical or horizontal, either disappears (if the size is small) or grows, turning into a spiral structure if its initial size is large enough.

In summary, in this section, we have shown that the SWS from Fig. 4 exhibits robustness against small deviations in shape and direction of motion allows us to assert that such an object really has spatiotemporal stability and can exist indefinitely.

3.4 Scaling reveals SWS family

The results above raise a natural question: how unique is the shape of the SWS we analyzed, and how structurally stable is it?

We conducted a series of computational experiments that showed that there are many variants of SWS of various size and speed. However, smaller SWSs, for which

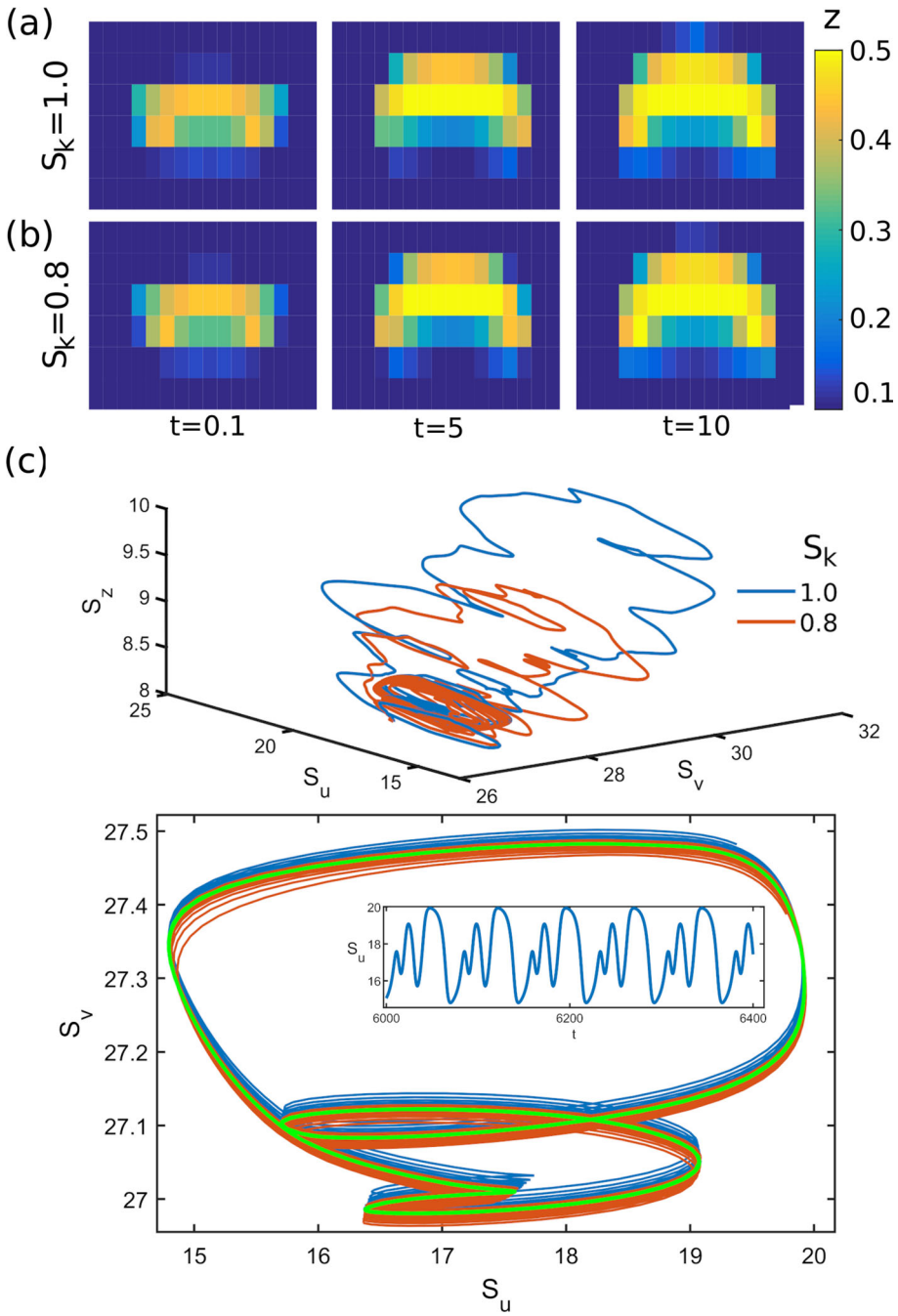

Fig. 5 Time evolution for **a** the original SWS ($S_k = 1.0$) and **b** the scaled SWS ($S_k = 0.8$); **c** 3D and 2D maps of the dynamics of sum values of u, v, z variables (for clarity we show the orbit in (Su, Sv) space after first 1000 arbitrary time units, we mark the final closed orbit by green color)

the discreteness of the model is more essential, exist in a wider range of diffusion rate γ_z. The spatial variation of γ_z reflects the spatial distribution of diffusivity, which is in good agreement with both biophysical reality and recent concepts about the diversity of diffusion processes, see, for example [36].

Figure 7 summarizes the obtained results. The initial SWS was scaled in two ways, either in all directions (thick lines), or only in the direction perpendicular to the direction of motion (thin lines). The evolution of S_z has revealed many stable variants, which can be seen as nearly constant (with small oscillations) level of S_z.

When scaling the original structure by a factor of S_k perpendicular to the direction of motion, for any considered $S_k > 1$, stable SWS appear after some rise of S_z. They always take the form of a flat front, rounded at the edges Small fluctuations of S_z over time reflect the oscillations of the SWS shape discussed above. Note once again that when scaling with the coefficients $S_k = 0.8$ and $S_k = 1.0$, the structures take the same final size.

In contrast, when initial conditions was set using scaling in both directions (see curves 2x, 3x, 4x), the evolution always starts with fall of S_z with subsequent stabilization. Visual inspection of the process reveals that

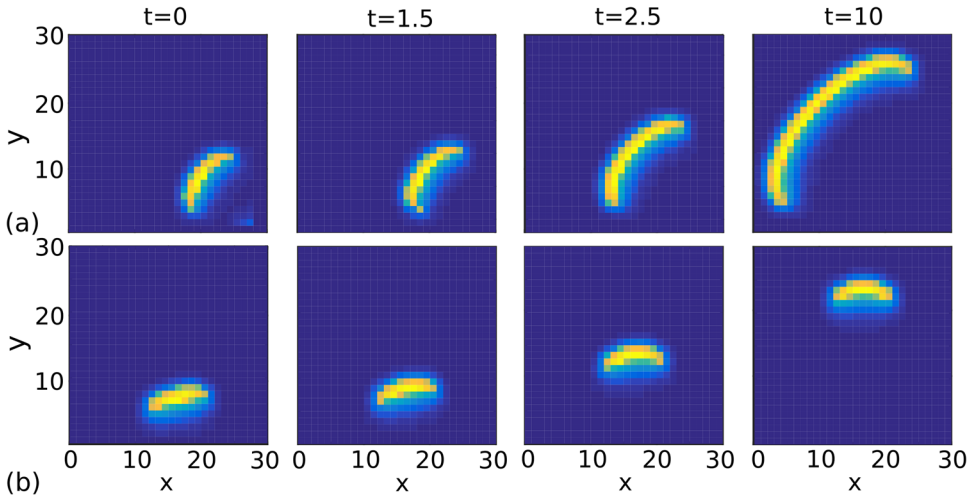

Fig. 6 Evolution of the shape of the structure obtained from the original **a** by a significant angle of rotation 45°, and **b** by a small angle 10°

initial shape first quickly becomes more thin, and then adjusts its size to be stable. Note, that resulted SWS is larger (have greater S_z) that SWS achieved with the same scaling factor but only in one direction.

All previous results were obtained with diffusion value $\gamma_z = 0.5$ (see Table 1). Our numerical experiments show that SWS can exist in a certain range of values of the diffusion coefficient γ_z.

As the size of the initial structure increases, the range of γ_z at which the SWS exists narrows: see Table 2, where S_k is a scaling factor in all directions. At values less than the lower value of the interval, the initial structures can not propagate and they disappear, at larger values they turn into a spiral wave. For the coefficients $S_k \geq 5$, we failed to find the γ_z values at which the initial conditions develop into the SWS.

Earlier, we demonstrated that SWS can only spread in a vertical or horizontal direction, so the velocity of pattern motion V_s determines the distance in pixels that SWS overcomes per unit of time in the direction of its motion. With the growth of SWS size, an increase in its velocity is observed as it is shown in Fig. 8. However, the velocity is limited by a certain value, to which the curve tends asymptotically with an increase in the SWS size. Below in Discussion we will argue that this limit coincides with the velocity of the infinitely wide flat wave at the given γ_z value.

Summarizing in this section, we have shown that by specifying different initial conditions, one can find a set of different variants of SWS, not necessarily of small size. Their common property is a small (3-5 pixels) thickness in the direction of motion, while the width can vary significantly. At the same time, the smallest (in width) SWS is slower than the wide ones.

3.5 SWSs persist in the randomized parameter landscape

The above discussed results were obtained using a regular 2D grid. Obviously, the arrangement of biological neurons is not so regular, see Fig. 1a. To demonstrate that our results are applicable to a more realistic medium, in this section, we consider nonhomogeneous solution domain. Specifically, we do not change the 2D mesh itself, but introduce a non-uniform distribution of parameters on it. To do so, the most suitable parameters are α_z and γ_z. The α_z parameter describes the rate of potassium outflow from neurons, so its spatial variability may account, for example, for the size of neurons. The heterogeneity of the distribution of the diffusion coefficient γ_z can describe the variable volume of the ECS between neurons. We consider the distribution of parameter values over the grid to be uniform over a certain interval with a mean value equal to the one for homogeneous case from Table. 1. An example of such a random deviation from the mean for the parameter γ_z is depicted in Fig. 9a.

The performed simulations show that SWSs remain stable even at a sufficiently large spread of parameters. The effect of γ_z inhomogeneity on a small SWS is shown in Fig. 9b. Similar graphs of changes in the shape of the edge of the large SWS, obtained from the original one by scaling 6 times perpendicular to the direction of motion, are shown in Fig. 9c. The top rows in (b) and (c) show the waveform at constant parameter values. Lower rows show the process of changing the waveform at 4 consecutive time moments with a step of 0.5.

We conclude that the inhomogeneity of the medium introduced by us leads only to small variations of the variables inside the wave region, not directly affecting

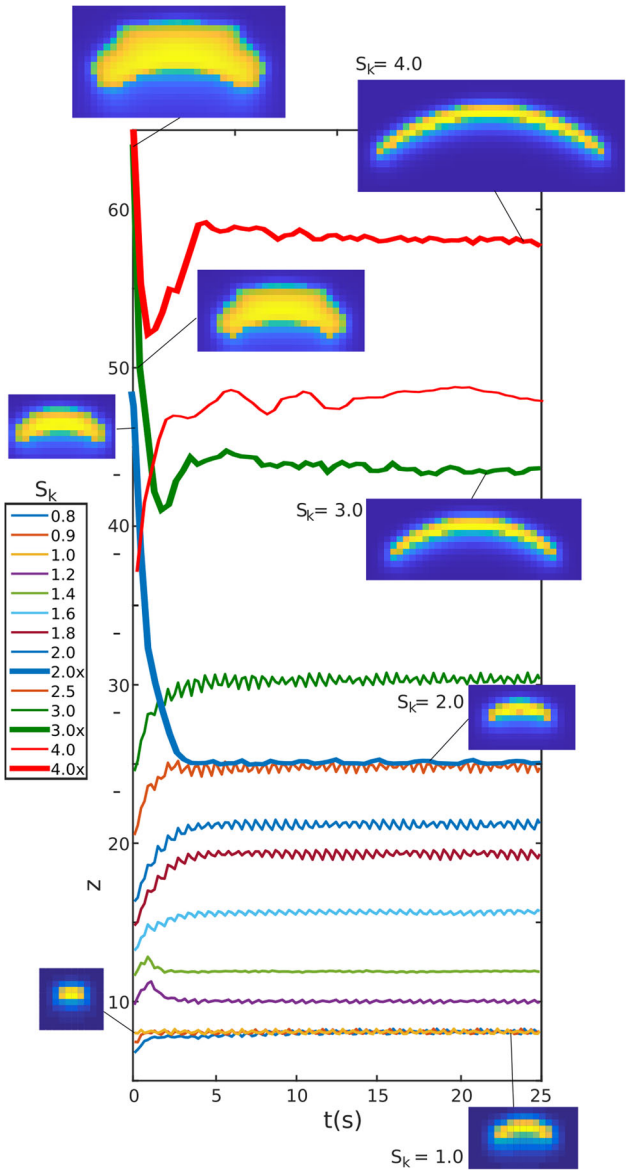

Fig. 7 Considerable scaling reveals multiple SWS variants. The initial conditions are obtained both by scaling the original structure (thick lines labeled as $S_k = 2.0$x at $\gamma_z = 0.45$, 3.0x at $\gamma_z = 0.408$, 4.0x at $\gamma_z = 0.403$; the notification kx means that the initial SWS was scaled in all directions in k times), and by expanding perpendicular to the direction of motion at $\gamma_z = 0.5$ (thin lines). Inserts in the left and right show the initial and final SWS shape, respectively

its stability. Note that large SWSs turned out to be more sensitive to medium inhomogeneity than small ones.

Thus, the existence of the SWSs under study is not a consequence of the regularity of the grid. This makes our results applicable for describing processes in real nervous tissue, in particular, for modeling stable wave fronts in migraine [18].

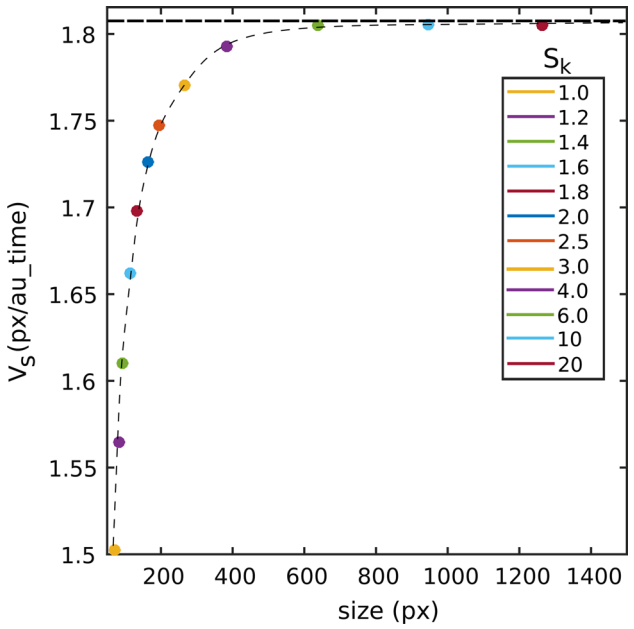

Fig. 8 Dependence of the SWS velocity on its size

Table 2 Diffusion intervals maintaining the SWS nature of the scaled structure

S_k	γ_z interval
1	0.479–0.683
2	0.425–0.460
3	0.405–0.411
4	0.402–0.404

4 Discussion

As we mentioned in Introduction, basic model of continuous excitable medium demonstrates fundamentally unstable behavior of isolated wave segments, for which negative feedback is usually used to stabilize [19, 37–39]. In contrast, our model medium demonstrates wave segments that are stable in time, insensitive to small changes in the initial conditions and exist at certain intervals of values of the model parameters.

To reveal the specific features of SWS that provide its stability, we have compared in detail the edges of structures with different widths. We found that while growing, SWS become more and more similar at the edges. The conclusion about the pivotal role of the SWS edges well correlates with the previously obtained results for a continuous medium, where the events in the boundary regions predetermine the instability of wave segments [38, 39].

Our results also expose that each of the considered SWS remain stable in a limited range of diffusion coefficient $\gamma \in (\gamma_{min}, \gamma_{max})$. At $\gamma < \gamma_{min}$ SWS decreases in sizes and vanishes, at $\gamma > \gamma_{max}$ it turns into an expanding wave front. Such behavior, together with the

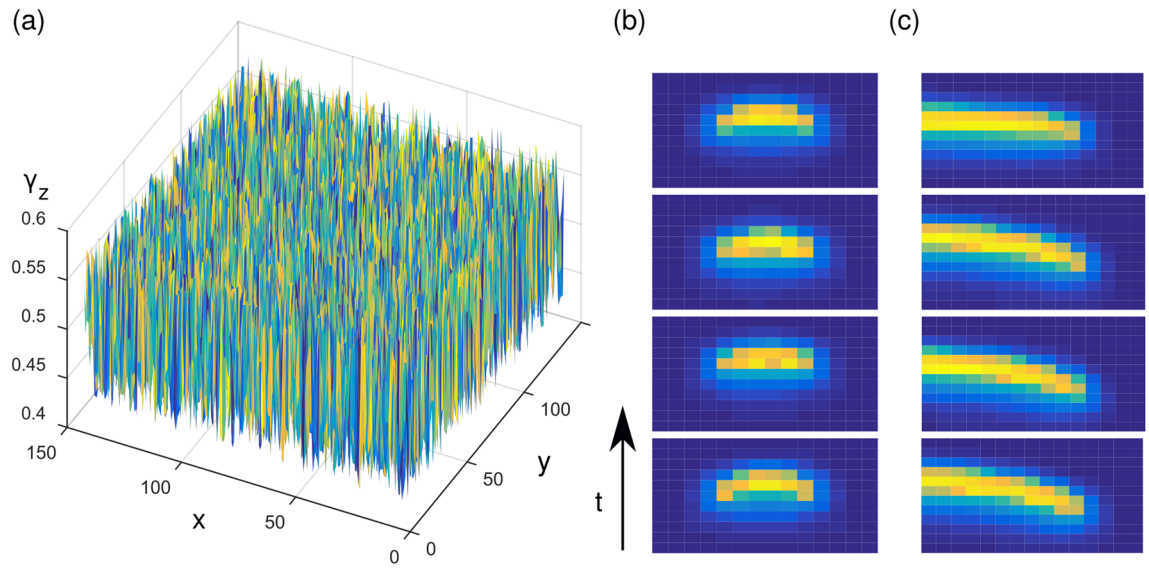

Fig. 9 SWS persists in a heterogeneous medium. **a** An example of the spatial distribution of the parameter γ_z; **b** dynamics of the variable z in the front of small sizes ($S_k = 1$); **c** dynamics of the variable z on one of the edges of the large front ($S_k = 6$). The solutions are given with a time step of 0.5, while in all cases the upper graphs show the shape of the structure for a uniform distribution of the parameter

properties that we mentioned above, allows us to propose a hypothesis about the mechanism underlying the existence of SWS.

One of the first reports on the effect of propagation failure in systems of discrete coupled cells was the study by Keener [40]. Later, this effect was studied both for bistable fronts in reaction-diffusion systems and for excitable systems [41–44]. Simplistically, we can say that excitation is not transmitted to the next discrete element, until some critical value of the activating factor is accumulated. In our case this factor is the amount of z.

Considering the events at the edge of the SWS, at each time step of the solution there are grid units where excitation can be transmitted and those where it cannot. The difficulty is that these exclusions and permissions change at every time step. Our hypothesis is that by finding SWS during the calculations in Sect. 3.1, we automatically find only those structures for which there is a periodicity in time: after a certain number of steps, they repeat themselves with a displacement in space. As our results show, a SWS is characterized by (i) a strictly flat central part and (ii) edges lagging behind the center. In this case, the shape of the edge does not have to be exactly specified, as we showed in Section 3.2, its small variations fade out. At the same time, a flat central part is critically needed, and violation of this condition will inevitably lead to an expanding wave, as in the Fig. 3a, right side. The minimum length of the flat part of a segment is 2 pixels, and such segments are most likely to occur. All other variants of structures will either disappear, or expand indefinitely, or evolve towards sustainable SWS, as we have shown in our work.

The oscillations of z sum in Fig. 4, 7 reflect such a repeating in time pattern. In our case, the criterion for whether a given grid unit can be excited or not is the amount of accumulated z in it. This, in turn, depends on both the diffusion coefficient and the state of neighboring elements, which changes in time.

In conclusion, we believe that the obtained results giving the new understanding of the processes in the nervous tissue will be useful, in particular, for the analysis of similar phenomena in case of spreading cortical depression, or activity patterns in migraine [45].

Along this way, the obvious next task is to generalize our results to irregular lattices. The grounds for optimism here are given by the stability of waves in non-homogeneous medium, since the heterogeneity of the parameter field and the unevenness of the location of the centers of activity are equivalent in a sense.

Supplementary Information The online version contains supplementary material available at https://doi.org/10.1140/epjs/s11734-023-00810-y.

Acknowledgements This research was supported by the Russian Science Foundation, project #22-15-00143 (sections 1, 2.1, 3.3, 3.4, 3.5, 4), and by the government of the Russian Federation, project #075-15-2022-1094 (sections 2.3, 3.1, 3.2,4).

Data availability This work has no associated data.

References

1. A.C. Charles, S.M. Baca, Nat. Rev. Neurol. **9**, 637 (2013)

2. J.P. Dreier, C.L. Lemale, V. Kola, A. Friedman, K. Schoknecht, Neuropharmacology **134**, 189 (2018)
3. K. Eikermann-Haerter, Headache **54**, 1146 (2014)
4. A.A. Leao, J. Neurophysiol. **7**, 359 (1944)
5. L.A.B.R.I. University of California, M.A.B. Brazier, Cortical excitability and steady potentials: relations of basic research to space biology. In *Proceedings of the First Conference, 1961. Editor: Mary AB Brazier* (University of California Press, 1963)
6. H.C. Tuckwell, R.M. Miura, Biophys. J. **23**, 257 (1978)
7. H. Kager, W.J. Wadman, G.G. Somjen, J. Neurophysiol. **84**, 495 (2000)
8. B.E. Shapiro, J. Comput. Neurosci. **10**, 99 (2001)
9. G. Somjen, H. Kager, W. Wadman, J. Comput. Neurosci. **25**, 349 (2008)
10. W. Yao, H. Huang, R.M. Miura, Bull. Math. Biol. **73**, 2773 (2011)
11. H. Tuckwell, *AIP Conference Proceedings*, vol. 1028, pp. 46-64 (2008) **1028**
12. M.A. Dahlem et al., Physica D Nonlinear Phenom. **239**, 889 (2010)
13. E. Santos et al., NeuroImage **99**, 244 (2014)
14. Z. Zheng, J. Luo, Z. Cao, S. Tan, J. Lv, J. Stroke Cerebrovasc. Dis. **31**, 106476 (2022)
15. M. Dahlem, E. Chronicle, Prog. Neurobiol. **74**, 351 (2004)
16. M.A. Dahlem, S.C. Müller, Annalen der Physik **13**, 442 (2004)
17. M.A. Dahlem, N. Hadjikhani, PloS One **4**, e5007 (2009)
18. M.A. Dahlem et al., Front. Comput. Neurosci. **9**, 29 (2015)
19. V. Zykov, K. Showalter, Phys. Rev. Lett. **94**, 068302 (2005)
20. A. Kenny, M.J. Plank, T. David, J. Theor. Biol. **472**, 11 (2019)
21. P.A. Arroyo, S. Alonso, R.W. dos Santos, Phys. Rev. E **97**, 032214 (2018)
22. S.A. Neymotin et al., Neural Comput. **27**, 898 (2015)
23. C. Iadecola, Neuron **96**, 17 (2017)
24. D. Postnov, F. Müller, R. Schuppner, L. Schimansky-Geier, Phys. Rev. E **80**, 031921 (2009)
25. D. Postnov, D. Postnov, L. Schimansky-Geier, Brain Res. **1434**, 200 (2012)
26. A. Verisokin, D. Verveyko, E.A. Kuryshova, D. Postnov, Chaos **28**, 106326 (2018)
27. E. Syková, C. Nicholson, Physiol. Rev. **88**, 1277 (2008)
28. J. Tønnesen, V.K. Inavalli, U.V. Nägerl, Cell **172**, 1108 (2018)
29. P.E. Kloeden, E. Platen, J. Stat. Phys. **66**, 283 (1992)
30. M. Khodabin, M. Rostami, Adv. Differ. Equ. **2015**, 1 (2015)
31. C. Rackauckas, Q. Nie, Discrete and continuous dynamical systems. Ser. B **22**, 2731 (2017)
32. D.E. Postnov, D.D. Postnov, R. Zhirin, The "AGEOM_CUDA" software for simulation of oscillatory and wave processes in two-dimensional media of arbitrary geometry on the basis of high-speed parallel computing on graphics processing unit technology CUDA, RF registration certificate #2012610085 from 10.01.2012. (in Russian) (2012)
33. F. Kneer, E. Schöll, M.A. Dahlem, New J. Phys. **16**, 053010 (2014)
34. N. Akhmediev, A. Ankiewicz, *Dissipative Solitons: From Optics to Biology and Medicine* (Springer, New York, 2008)
35. M. Yu et al., Nat. Commun. **8**, 1 (2017)
36. R. Metzler, A.V. Chechkin. arXiv:2204.01048 (2022)
37. V. Zykov, Eur. Phys. J. Spec. Top. **157**, 209 (2008)
38. V. Zykov, E. Bodenschatz, New J. Phys. **16**, 043030 (2014)
39. V.S. Zykov, E. Bodenschatz, Phys. Rev. E **97**, 030201 (2018)
40. J. Keener, Siam J. Appl. Math. **47** (1987)
41. T. Erneux, G. Nicolis, Physica D Nonlinear Phenom. **67**, 237 (1993)
42. A. Hagberg, E. Meron, Phys. Rev. E **57**, 299 (1998)
43. G. Fáth, Physica D Nonlinear Phenom. **116**, 176 (1998)
44. N. Kouvaris, T. Isele, A. Mikhailov, E. Schöll, EPL **106**, 68001 (2014)
45. M. Dahlem, T. Isele, J. Math. Neurosci. **3**, 7 (2013)